Role of elastic exciton-defect scattering in resonant Raman and resonant Brillouin scattering in CdSe

Claudine Hermann* and Peter Y. Yu†
IBM Thomas J. Watson Research Center, Yorktown Heights, New York 10598
(Received 13 November 1979)

We report a detailed resonant Brillouin and Raman study in the wurtzite semiconductor CdSe in the vicinity of its lowest-energy A exciton. By using a spectrometer and laser system with a combined spectral resolution of 0.16 cm^{-1} we were able to measure the widths and line shapes of Raman and Brillouin modes. In a nominally undoped CdSe sample we found that wave vector is conserved in the light-scattering process only for incident photon frequencies below the longitudinal exciton frequency. For incident laser frequencies above the longitudinal exciton frequency, scattering processes which do not conserve wave vector became dominant. We propose that this breakdown in wave-vector conservation is due to elastic exciton-defect scattering, and our results are in qualitative agreement with the predictions of the elastic exciton-defect scattering theory of Gogolin and Rashba. In another CdSe sample doped with Li, we found that its Raman and Brillouin spectra are always dominated by wave-vector-nonconserving modes even for incident photon frequencies below the A-exciton frequency. From the Brillouin spectra we deduced the following parameters for the A exciton in CdSe: $M_\perp$ (exciton mass perpendicular to the c axis) $= 0.40m_0$ (free electron mass), $M_\parallel \sim 1.3m_0$, ω_T (transverse exciton frequency) $= 14713$ cm^{-1} (at ~ 10 K), and the splitting between longitudinal and transverse exciton frequencies is 4 cm^{-1}.

I. INTRODUCTION

The influence of defects on nonresonant Raman scattering in solids has been investigated extensively.[1] In general defects modify the Raman spectra of a solid in two ways. Defects introduce new vibrational and electronic Raman modes which are absent in the perfect crystal. Such defect-induced Raman modes are not the subject of this paper. Defects also change the line shape and intensities of the Raman modes of the perfect crystal.[2] To observe these effects a fairly high defect concentration ($\gtrsim 10^{18}$ cm^{-3}) is usually necessary. However, in resonant Raman scattering defect effects become observable at much lower concentrations.[3]

Recently the role of impurities in resonant Raman scattering in semiconductors has been studied. Several authors[4] have shown that excitons bound to impurities form resonant intermediate states in Raman scattering. Yu and Shen[5] showed that impurities can broaden and shift the E_1 resonance peak in the Raman cross section of optical phonons in InSb. Permogorov and Reznitsky[6] have studied the effect of Ni on momentum conservation in resonant Raman scattering in CdS. Ulbrich and Weisbuch[7] suggested that impurities are important in the resonant Brillouin scattering of exciton polaritons in GaAs. In comparison there are relatively few theoretical studies of impurity effects in resonant Raman scattering in semiconductors.[8] Recently Gogolin and Rashba[9] showed that defects, even in low concentrations, can contribute significantly to the resonant Raman scattering of LO phonons due to elastic exciton-defect scatterings.

In this paper we report a study of resonant Raman and resonant Brillouin scattering in CdSe samples doped with different concentrations of impurities. By using a cw dye laser and spectrometer system whose combined spectral width is ~0.16 cm^{-1}, we are able to observe defect-induced changes in the line shapes of the Raman and Brillouin spectra of CdSe when excited resonantly. We obtain for the first time direct evidence of elastic exciton-defect scattering predicted by Gogolin and Rashba.

The organization of this paper is as follows. In Sec. II we summarize the theories of resonant Raman and resonant Brillouin scattering via excitons, both with and without the effect of exciton-defect scattering. In Sec. III the electronic and vibrational properties of CdSe are presented, including the selection rules for Brillouin and Raman scatterings. The experimental setup and sample properties are given in Sec. IV. The experimental results and their interpretations are presented in Sec. V. Section VI summarizes the results and conclusions of this article.

II. THEORY OF RESONANT RAMAN AND RESONANT BRILLOUIN SCATTERING VIA EXCITONS

A. Neglecting defects

The theory of resonant Raman scattering via excitons in semiconductors, neglecting the effect of defects, has been treated extensively in the literature.[10] The corresponding theory of resonant Brillouin scattering has been studied by Brenig *et al.*[11] We will briefly summarize these theoreti-

cal results as an introduction to the theory of Gogolin and Rashba[9] which includes exciton-defect scattering.

We assume a model system consisting of only photons and a semiconductor with one single exciton band and several phonon branches (both acoustic and optical phonons). Furthermore, we assume the exciton dispersion to be parabolic:

$$\hbar\omega_{ex}(\vec{k}) = \hbar\omega_{ex}(0) + \hbar^2 k^2/2M \,, \tag{1}$$

where M is the exciton effective mass and $\hbar\vec{k}$ is the crystal momentum of the exciton. In the rest of this paper momentum will always mean crystal momentum.

In the absence of defects there are only two interactions which are important for light scattering inside the semiconductor. These are the exciton-photon interaction (H_{ER}) and the exciton-phonon interaction (H_{EP}). The different exciton-phonon interaction mechanisms which can be studied by light scattering have been reviewed recently by Yu.[12] Both acoustic and optical phonons interact with excitons by the deformation potential mechanism. In noncentrosymmetric crystals the longitudinal-optical (LO) phonon can couple to excitons via an additional Fröhlich interaction. In piezoelectric crystals the acoustic phonons have an additional piezoelectric exciton-phonon interaction. Both the Fröhlich and piezoelectric interactions depend on the phonon wave vector while the deformation potential interactions are wave-vector independent.

The exciton-photon interaction leads to the formation of a coupled mode known as the exciton polariton inside the medium. It has been shown by many authors that the exciton-polariton dispersion is given by[11,13,14]

$$\frac{c^2k^2}{\epsilon_0\omega^2} = 1 + \frac{\omega_L^2 - \omega_T^2}{\omega_T^2 + (\hbar k^2\omega_T/M) - \omega^2 - i\omega\Gamma} \,. \tag{2}$$

In Eq. (2), ω_T [$=\omega_{ex}(0)$] and ω_L are, respectively, the transverse and longitudinal exciton frequencies, ϵ_0 is the background dielectric constant of the medium without the exciton contribution, c is the speed of light, and Γ is the damping of the exciton. If Γ is assumed to be zero, Eq. (2) can be solved easily to give the two polariton branches shown schematically in Fig. 1(a). These two branches will be labeled 1 and 2, respectively. For polariton energy well below $\hbar\omega_T$, branch 2 is photonlike. For polariton energies well above $\hbar\omega_L$ branches 1 and 2 resemble, respectively, the uncoupled photon and exciton. Only in the vicinity of $\hbar\omega_T$ and $\hbar\omega_L$ are the exciton and photon strongly coupled together.

If Γ is not zero the nature of the solutions of Eq. (2) can change drastically with Γ. Tait[14] has

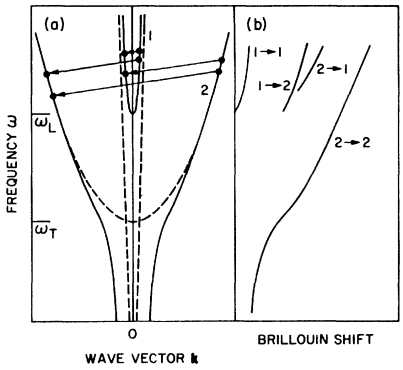

FIG. 1. (a) Schematic polariton dispersion curves showing the four Brillouin-scattering processes (indicated by arrows) proposed by Brenig, Zeyher, and Birman. The broken curves show the dispersion of the uncoupled photon and exciton. (b) Schematic dependence of the Brillouin shifts on polariton frequency for the four Brillouin processes shown in (a). The notation 1 → 2 represents the Brillouin scattering of a polariton from branch 1 to branch 2. ω_T and ω_L are, respectively, the transverse and longitudinal exciton frequencies.

defined a value Γ_c by

$$\Gamma_c = 2\left[2\hbar\omega_T^2(\omega_L - \omega_T)/(Mc^2)\right]^{1/2} . \tag{3}$$

For $\Gamma \lesssim \Gamma_c$ the polariton dispersion curves are essentially the same as in the case $\Gamma = 0$. However, for Γ larger than Γ_c the photon becomes decoupled from the exciton and the polariton dispersion approaches those of the uncoupled exciton and the photon [shown as the broken curves in Fig. 1(a)].

There are many advantages in using the exciton-polariton concept to describe resonant light scattering in semiconductors. Since the polariton wave functions are already diagonal in the exciton-photon interaction, the only interaction Hamiltonian left is the exciton-phonon interaction. In most semiconductors this interaction is weak enough to be treated perturbatively. Since in the polariton picture inelastic scattering of light becomes simply inelastic scattering of polaritons by phonons, the scattering cross section can be calculated easily using the "golden rule." The polariton picture is still valid for $\Gamma > \Gamma_c$ when the exciton and photon become decoupled.

The theory of Brillouin scattering of polaritons was first proposed by Brenig *et al.*[11] These authors pointed out that, for a given acoustic phonon branch, as many as four polariton-phonon scattering processes are possible in the vicinity of ω_L. These four processes are shown by arrows in Fig. 1(a). These four Brillouin processes can be distinguished from each other by the different dependence of their frequencies on polariton energy

as shown in Fig. 1(b). The widths of these Brillouin modes also depend differently on polariton energy. These polariton-phonon scattering processes have recently been observed in several semiconductors.[15]

Resonant Raman scattering of polaritons has been studied theoretically by many authors.[16-19] The optical phonon frequency is usually much larger than the splitting $\omega_L - \omega_T$ so when the incident polariton frequency ω_i is in the vicinity of ω_L the scattered polariton frequency ω_s would be well below ω_T. Therefore unlike Brillouin scattering, there are only two polariton Raman scattering processes. These are shown schematically in Fig. 2(a). Also the optical phonons usually have very small dispersion compared to the acoustic phonons, so these two processes cannot be distinguished by the dependence of their Raman frequencies on polariton energy. However, their scattering cross sections do have different dependence on polariton energy. As pointed out by Bendow and Birman[18] and by Verlan and Ovander[17] the $2 \rightarrow 2$ Raman process dominates for ω_i below ω_T. Its scattering efficiency increases with ω_i approximately as $(\omega_i - \omega_T)^{-1}$, for $\omega_i < \omega_T$, peaks slightly below ω_T, and then decreases for $\omega_i > \omega_L$. The decrease above ω_L reflects the smaller conversion efficiency of external photons to branch 2 polaritons above ω_L. On the other hand, the $1 \rightarrow 2$ Raman process is negligible for $\omega_i \lesssim \omega_T$. Its scattering efficiency peaks around ω_L and dominates over the $2 \rightarrow 2$ process for ω_i above ω_L. If the exciton-phonon interaction is wave-vector independent the maximum scattering efficiencies for both processes are comparable. But if the exciton-photon interaction is wave-vector dependent, the $2 \rightarrow 2$ process is more favorable than the $1 \rightarrow 2$ process. This is because the phonon emitted in the $2 \rightarrow 2$ process has a much larger wave vector as shown in Fig. 2(a). Gogolin and Rashba[9] pointed out that under such circumstances the two-phonon (LO phonon plus an acoustic phonon) process shown in Fig. 2(b) may become more favorable than the one-phonon processes because the LO phonon emitted now can have larger wave vectors. The two-phonon process would be particularly favorable in strongly piezoelectric crystals because the piezoelectric exciton-acoustic phonon interaction is also wave-vector dependent. Recently, Koteles and Winterling[20] have observed these two-phonon modes in CdS when they tuned ω_i above ω_L. Furthermore, the dependence of the frequencies of these two-phonon modes on incident photon energy indicates that the exciton-acoustic phonon interaction is indeed due to the piezoelectric interaction.

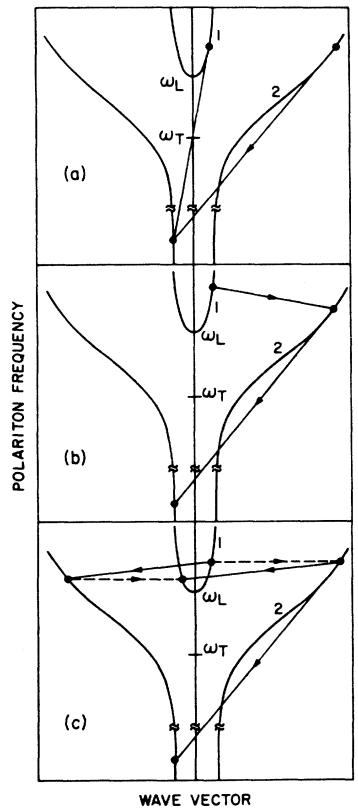

FIG. 2. (a) Schematic representations of two Raman scattering processes of polaritons. (b) Schematic representation of a two-phonon scattering of polariton in which a polariton in branch 1 is scattered to branch 2 with emission of an acoustic phonon followed by the scattering of the branch 2 polariton with emission of an LO phonon. (c) Schematic representation of Raman and Brillouin scattering of polaritons involving elastic exciton-impurity scattering. The broken arrows denote elastic exciton-impurity scatterings. Two Brillouin processes are shown. In one, the polariton is first elastically scattered from branch 1 to branch 2 and then scattered back to branch 1 with emission of an acoustic phonon. In the second process, the two steps are reversed. In the Raman process, the polariton is scattered elastically from branch 1 to branch 2 and then from branch 2 back to branch 2 with emission of an LO phonon.

B. Including effect of defects

Defects can affect resonant light scattering in a semiconductor in several ways. Defects can trap excitons to form bound excitons. These bound excitons then form resonant intermediate states in the scattering process.[4] Defects can also scatter excitons elastically or inelastically. These scattering processes contribute to the exciton damping Γ. As pointed out in Sec. II A, the polariton dispersion depends on Γ so the Brillouin spectra which are sensitive to the polariton dispersion are

effected by defects. In inelastic exciton-defect scattering the exciton loses energy in exciting the defect into an electronic or vibrational excited state. This results in new peaks in the Raman spectra. In elastic scattering the exciton energy is unchanged but its wave vector is altered. If these elastically scattered excitons emit a phonon before radiative recombination, momentum is not conserved in the resultant Raman or Brillouin process because the momentum of the scattered phonon is no longer equal to the momentum difference between the incident and scattered photons. The extra momentum is taken up by the defect. In this paper we are interested mainly in the elastic exciton-defect scatterings. Inelastic scatterings which produce defect-induced Raman modes will be the subject of a separate paper.[21]

The theory of elastic scattering between impurities and excitons has been studied by several authors.[9,22,23] Recently, Gogolin and Rashba[9] applied these theories to resonant Raman scattering of LO phonons. Here we will present some of the important conclusions of their theory. Gogolin and Rashba pointed out that if the exciton-phonon scattering is wave-vector dependent, such as for LO phonons, the $1 \rightarrow 2$ scattering process in Fig. 2(a) is not very strong because of the small phonon wave vector involved. In the presence of defects the polariton in branch 1 can be scattered elastically into branch 2 by collision with defects. Once the polariton is in branch 2 it can emit an LO phonon with much larger wave vector, as shown in Fig. 2(c). This process is similar to the two-phonon process shown in Fig. 2(b) except that exciton-defect scattering replaces the exciton-acoustic phonon scattering. In fact, the two processes compete with each other with the defected induced process dominating in heavily doped samples. Although Gogolin and Rashba applied their theory to LO-phonon scattering, their theory is valid also for the piezoelectric acoustic phonons. The corresponding Brillouin processes including elastic exciton-defect scattering are shown also in Fig. 2(c). To distinguish these Brillouin and Raman modes, which result from elastic exciton-defect scattering, from the ones not involving defects we shall denote them as LO*, LA*, and TA*.

The defect induced modes have several features which distinguish them from the normal modes not involving defects. First, momentum is *not* conserved in the scattering processes involving defect scattering in the sense that the phonon wave vector $\vec{q}$ is not equal to the difference between the incident and scattered photon wave vectors. From Fig. 2(c) it is clear that the phonon wave vector is approximately equal to the wave vector of the branch 2 polariton which is the resonant intermediate state. This breakdown in momentum conservation affects the Raman and Brillouin modes differently. In the case of the LO* mode, the effects are usually not very prominent. In case the exciton and LO-phonon dispersions are isotropic as in a cubic crystal, the LO*-phonon band is no different from the LO-phonon band except in intensity. In anisotropic crystals such as CdS and CdSe, the breakdown in momentum conservation can modify the selection rules and cause drastic changes in the LO-phonon line shape. The Brillouin modes are affected to a greater extent by momentum nonconservation because of the linear acoustic phonon dispersion. In general, we expect the TA* and LA* bands to be broader (depending on the anisotropy of the exciton dispersion). Their peak positions will vary with the incident photon energy as in the case of Brillouin scattering by polaritons in the absence of defects. However, their frequencies will not be the same as the moment-conserving modes. Second, the momentum-nonconserving modes are important only when the incident photon frequency is above ω_L when branch 1 polaritons are excited. Also, we expect the intensity of these defect-induced modes to increase with defect concentration.

We should also point out some differences between the momentum-nonconserving modes LO*, TA*, and LA* discussed here and the momentum-nonconserving modes discussed in Ref. 2. In Ref. 2, the samples studied have such high defect concentration that momentum is no longer a good quantum number. In those cases, phonons with a large range of wave vectors are excited and the resultant Raman peaks tend to be very broad and reflect the phonon density of states. These phonons do not necessarily have a wave-vector dependent exciton-phonon interaction and they can be observed in off-resonance. In the present case, only phonons with a limited range of wave vectors are observed because they are selectively enhanced by the resonant exciton intermediate state. Thus the LO*, LA*, and TA* modes are best studied in samples which are lightly doped with impurities. That is, the concentration of impurities is high enough to make exciton-impurity scattering significant but not high enough to cause complete breakdown in momentum conservation. Theoretically, it is possible to calculate the optimal concentration of impurities for observing the LO*, LA*, and TA* modes if the impurity potential is known.[9] In practice, it means the sample should have an exciton damping $\Gamma \lesssim \Gamma_c$.

Resonant light scattering via bound excitons has also been studied by Gogolin and Rashba by assuming that the impurity-exciton potential contains one bound state. Due to the localization of the ex-

citon around the impurity, the emitted phonon can have a range of wave vectors. Hopfield,[24] for example, showed that for piezoelectric acoustic phonons, the bound exciton couples most strongly to phonons with wave vector given approximately by $(r_e + r_h)^{-1}$, where r_e and r_h are respectively the distance between the impurity and the electron and between the impurity and the hole. Thus momentum is not conserved also in resonant light scattering via bound excitons, the phonon momentum being determined by the localization of the bound exciton around the impurity. Resonant Raman scattering at bound excitons has been studied in CdS by Colwell and Klein and by Damen and Shah. Resonant Brillouin scattering at bound excitons has been reported by us in CdSe.[25]

III. ELECTRONIC AND VIBRATIONAL PROPERTIES OF CdSe

The electronic properties of CdSe have been studied extensively by reflectivity, absorptivity,[26-29] and photoluminescence.[30-32] It is well established that the lowest conduction-band minimum in CdSe occurs at the Brillouin-zone center with symmetry Γ_7 (a discussion of the irreducible representations in wurtzite crystals can be found in Ref. 33). The valence-band maxima also occur at the zone center and have symmetries Γ_9, Γ_7, and Γ_7 in the order of decreasing energy. The excitons formed by these three valence bands and the conduction band are known as the A, B, and C excitons, respectively. In this paper we are concerned mostly with the lowest-energy A exciton. The $1s$ ground-state symmetries of the A exciton are Γ_5 and Γ_6. The Γ_6 state is electric-dipole forbidden and therefore is not important in this work. The Γ_5 exciton is electric-dipole allowed for radiation polarized perpendicular to the crystal's c axis (to be denoted by $\vec{E} \perp \hat{c}$) and gives rise to an exciton polariton. The dispersion of this polariton in CdSe has been determined by Kiselev *et al.*[34] using reflectivity measurements in very thin CdSe samples. The exciton parameters, in Eq. (2), they obtained are[34] $\epsilon_0 = 8.4 \pm 0.3$, $M_\perp = 0.41 \pm 0.02 m_0$ (m_0 being the free-electron mass), $\omega_L - \omega_T = 7.7 \pm 1$ cm^{-1}, $\omega_T = 14\,722.2$ cm^{-1}, and $\Gamma = 0.5 \pm 0.2$ cm^{-1}.

Bound excitons in CdSe have been studied by Henry *et al.* in photoluminenscence.[32] The frequencies of the A exciton in CdSe bound to neutral donors and acceptors are, respectively, 14 694.8 cm^{-1} (known as the I_2 bound exciton) and 14 657 cm^{-1} (known as the I_1 bound exciton).

The large absorption cross section of Cd atoms for thermal neutrons has impeded the determination of the phonon dispersions in CdSe by neutron scattering. Only the frequencies of its zone-center optical phonons have been reported recently by Plotnichenko *et al.*[35] Their room-temperature results are listed in Table I. The acoustic-phonon velocities in CdSe calculated from the elastic constants[36] are 1.54×10^5 cm sec^{-1} (transverse mode) and 3.57×10^5 cm sec^{-1} (longitudinal mode).

The selection rules for Raman and Brillouin scattering in CdSe have been reported by several authors.[37] For small phonon wave vectors ($q \sim 0$) the nonzero elements of the Raman tensors are (the z axis is chosen to coincide with the c axis)

$$\Gamma_6 \qquad \Gamma_1(z) \qquad \Gamma_5(x,y)$$

$$\begin{pmatrix} d & d & 0 \\ d & -d & 0 \\ 0 & 0 & 0 \end{pmatrix} \quad \begin{pmatrix} a & 0 & 0 \\ 0 & a & 0 \\ 0 & 0 & b \end{pmatrix} \quad \begin{pmatrix} 0 & 0 & c \\ 0 & 0 & c \\ c & c & 0 \end{pmatrix}$$

In our experiment we use a backscattering geometry with both incident and scattered photon wave vectors parallel or perpendicular to the c axis ($\vec{k} \parallel \hat{c}$ or $\vec{k} \perp \hat{c}$). The photon polarizations are always perpendicular to the c axis in order that the A exciton is the dominant intermediate state. The allowed Raman modes in CdSe deduced from the above Raman tensor are Γ_6, Γ_1 (TO) for $\vec{k} \perp \hat{c}$, and Γ_6, Γ_1 (LO) for $\vec{k} \parallel \hat{c}$. It is well known that in resonant Raman scattering via excitons, wave-vector-dependent scattering of the LO phonon can be important.[10] This will result in the Γ_5 (LO) phonon being present in the $\vec{k} \perp \hat{c}$ configuration.

The selection rule for Brillouin scattering in CdSe can be deduced from its elasto-optical tensors.[38] For both $\vec{k} \perp \hat{c}$ and $\vec{k} \parallel \hat{c}$ the allowed Brillouin mode is the LA phonon. In piezoelectric crystals such as CdSe, the possibility of wave-vector-dependent Brillouin scattering has to be considered. As has been shown in CdS, the TA phonon can be observed in the $\vec{k} \perp \hat{c}$ configuration due to wave-vector-dependent scattering.[39]

In summary, the phonons which can be observed in our scattering geometries are listed in Table II.

IV. EXPERIMENTAL SETUP AND SAMPLE CHARACTERISTICS

The Raman and Brillouin spectra of CdSe have been obtained with a conventional Raman scat-

TABLE I. Results of Plotnichenko *et al.* (Ref. 35) for the frequencies of zone-center optical phonons in CdSe at room temperature.

Mode	Frequencies (cm^{-1})
Γ_6 or E_2	34
Γ_5 or E_1 (LO)	211
Γ_1 or A_1 (LO)	209
Γ_5 or E_1 (TO)	169
Γ_1 or A_1 (TO)	166

TABLE II. The allowed Raman and Brillouin modes in CdSe when effects of elastic exciton-defect scattering are neglected. The scattering configurations are incident and scattered photons polarized perpendicular to the c axis; the photon wave vector $\vec{k}$ is either parallel or perpendicular to the c axis.

Configuration	Wave-vector-independent scattering	Wave-vector-dependent scattering
$\vec{k} \parallel \hat{c}$	Γ_6, Γ_1 (LO), LA	Γ_1 (LO)
$\vec{k} \perp \hat{c}$	Γ_6, Γ_1 (TO), LA	Γ_5 (LO), TA

tering setup with slight modifications. The excitation source is a Coherent Radiation Inc. Model 590 dye laser (dyes: Cresyl Violet or Rhodamine B) pumped by the 514.5-nm output of an Ar-ion laser. The dye laser linewidth is narrowed to less than 0.1 cm^{-1} by a 0.5-mm-thick intracavity étalon. Because the overall resolution of the system is limited by the spectrometer rather than by the dye laser, no attempt was made to make the dye laser single mode. The unwanted fluorescence from the dye laser is removed with a holographic grating. The dye laser beam is focused onto the sample with a spherical lens in a backscattering geometry. Using a spherical lens rather than a cylindrical lens results in some sample heating. With a smaller focus on the sample it is easier to find a smooth spot on the sample which scatters less light elastically. The sample is cooled by He exchange gas. Sample heating is minimized by keeping the dye-laser power below 3 mW. The sample temperature at the laser focal spot is estimated to be $\lesssim 10$ K by comparing the luminescence spectra with those measured at ~2 K by immersing the sample in superfluid He. The scattered radiation is analyzed by a 0.87-m Spex double monochromator with 1800-lines/mm holographic gratings. With a slit width of 25 μm, the spectral width of the spectrometer is determined to be 0.16 cm^{-1}. The scattered photons are detected by a cooled photomultiplier and a photon-counting system.

We have studied several CdSe samples grown by different techniques at several laboratories. Most of the heavily doped samples have a strong background (due to luminescence and elastic scattering), which masks the Brillouin peaks. We have observed resonantly enhanced Brillouin scattering in only two CdSe samples and most of the results reported here have been obtained from these two samples.

The first sample is nominally undoped and will be denoted by CdSe-P. It is a thin platelet grown from the vapor phase with the c axis contained in the sample face. The sample surface is mirror-like and is measured as grown. The size of the sample (~1×2 mm^2) is too small for impurity analysis by spark-source mass spectrometry. The sample quality is estimated from its luminescence and off-resonant Raman spectra shown, respectively, in Figs. 3 and 4. The luminescence spectrum shows a sharp I_2 peak (exciton bound to unidentified neutral donors) at 14 696 cm^{-1} and no

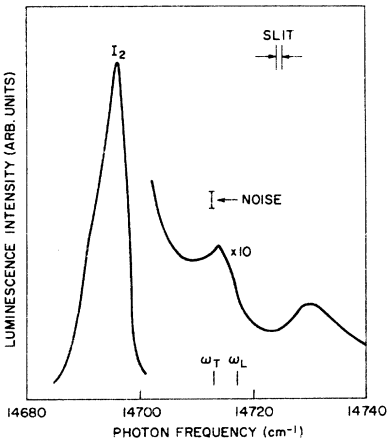

FIG. 3. Photoluminescence spectrum of CdSe-P with photons polarized perpendicular to the c axis. I_2 denotes a bound exciton peak.

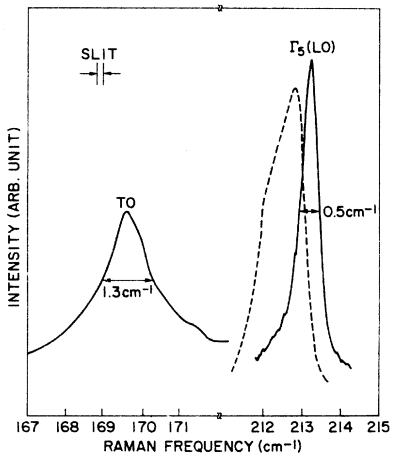

FIG. 4. Off-resonant Raman spectrum of CdSe-P. The excitation frequency is 14 618.3 cm^{-1} and the scattering configuration is $\vec{E} \perp \hat{c}$ and $\vec{k} \perp \hat{c}$. The broken curve is obtained from the 2LO-phonon spectrum by scaling down the Raman frequency by a factor of 2 and is meant to represent the LO-phonon density of states.

traces of I_1 peaks. The Raman spectrum of this sample shows sharp one-phonon peaks as predicted by our selection rule. In particular, we note that the Γ_5 (LO) phonon at 213.2 cm^{-1} in Fig. 4 is quite sharp and there is no sign of any impurity induced Γ_1 (LO) phonon at 212.3 cm^{-1}. We have also measured the reflectivity spectrum of this sample and observed a strong dip associated with the A-exciton polariton. These results all indicate that CdSe-P is of fairly high quality with low impurity concentration. The broken curve in Fig. 4 is obtained from the 2LO Raman peak by scaling down its Raman frequency by a factor of 2. In many group IV and III-V semiconductors it has been shown that such "reduced" 2LO spectrum reflects quite well the LO-phonon density of states.[40] We note that the broken curve in Fig. 4 has a cutoff at the Γ_5 (LO)-phonon frequency and a shoulder at the frequency of the Γ_1 (LO) phonon. This is consistent with our assumption that the broken curve represents the LO-phonon density of states in CdSe.

The second CdSe sample is a bulk sample grown from the melt and doped with Li. It will be denoted by CdSe-L. In this case, the sample surfaces are prepared by cleaving. Its dominant impurities and their concentrations are determined by spark-source mass spectrometry to be Li(1.4×10^{19} cm^{-3}) and Cl(1×10^{17} cm^{-3}). Lithium is amphoteric in CdSe while Cl is a shallow donor. Figure 5 shows part of the luminescence spectrum of this sample (at ~2 K). It is dominated by a strong I_1 peak at 14 659 cm^{-1} and an I_2 peak at 14 699 cm^{-1}. The reflectivity spectra of this sample at the A exciton have a line shape typical of a "bare" exciton rather than a polariton. The off-resonant LO-phonon Raman spectra of CdSe-L are shown in Fig. 6 for both $\vec{k}\parallel\hat{c}$ and $\vec{k}\perp\hat{c}$. We note that unlike the purer CdSe-P sample, the $\vec{k}\perp\hat{c}$ spectrum in CdSe-L is dominated by the Γ_1 (LO) phonon which is normally not allowed even by wave-vector-dependent scattering. These spectra will be discussed in more detail later.

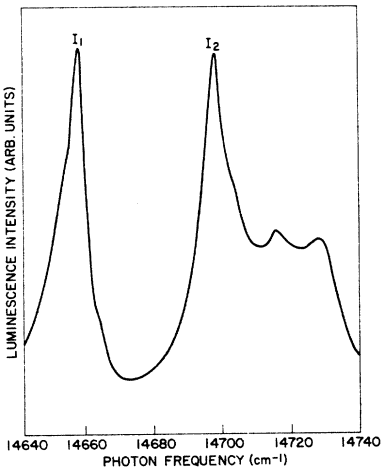

FIG. 5. Photoluminescence spectrum of CdSe-L showing the I_1 and I_2 bound exciton peaks.

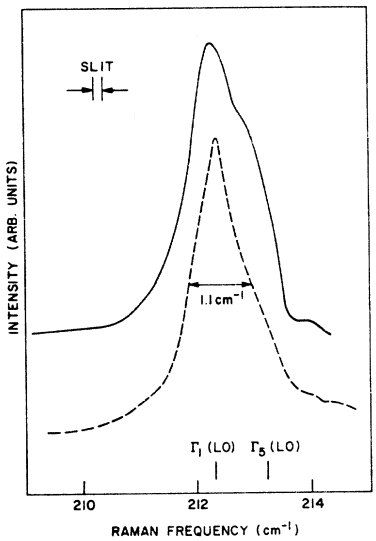

FIG. 6. Raman spectra of CdSe-L excited at laser frequency 14 719.1 cm^{-1} for two different scattering geometries: $\vec{E}\perp\hat{c}$ (solid curve) and $\vec{E}\perp\hat{c}$ and $\vec{k}\parallel\hat{c}$ (broken curve).

Finally, for comparison purpose, we present the Raman spectrum of a third CdSe sample (Fig. 7). This is a bulk sample purchased from Eagle-Picher. Enhancements of its Raman modes at free and bound excitons and at donor-acceptor pair recombination peaks have been reported in previous publications.[41] Spark-source mass-

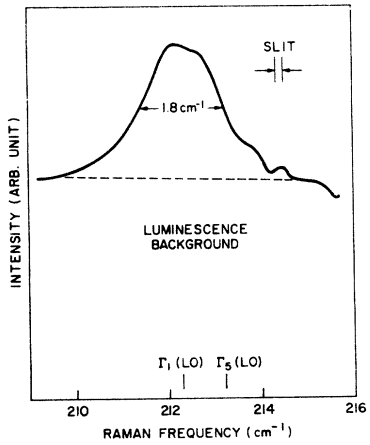

FIG. 7. Raman spectrum of a bulk CdSe sample purchased from Eagle-Picher. The excitation frequency is 14 652.5 cm^{-1}. The width of the LO-phonon peak in this sample is considerably larger than in the other CdSe samples.

spectrometry analysis indicated that it contains no known shallow acceptors or donors other than Na in amounts larger than 10^{16} cm^{-3}. Its luminescence spectra is dominated by one broad peak at 14 675 cm^{-1}, which is probably due to excitons bound to some unidentified donor levels. As seen from Fig. 7, the LO-phonon peak in this sample is broader than in the other two samples. Furthermore, the line shape of the LO phonon remains unchanged when the excitation frequency is varied. These results suggest that the amount of disorder in this sample is so large that momentum is always not conserved in the Raman process.

V. RESULTS AND DISCUSSIONS

A. Resonant Brillouin scattering in CdSe-*P*

We first present the resonant-Brillouin-scattering results in the CdSe-*P* sample and from these results determine the polariton dispersion in CdSe.

In CdSe-*P* we observed two low-frequency peaks in the scattered spectra ($\vec{k} \perp \hat{c}$ and $\vec{E} \perp \hat{c}$). The frequencies and widths of these peaks vary with the excitation frequency ω_1 (as shown in Figs. 8 and 9) similar to what was reported in CdS. Based on the CdS results we identified these peaks as due to scattering of the polariton by the TA and LA phonons in CdSe (crosses and solid circles in Fig. 8). Using the acoustic-phonon velocities of CdSe given in Sec. III, we fitted the experimental points (closed circles and crosses) in Fig. 8 with Eq. (2) by varying all the parameters except Γ which is assumed to be zero. The theoretical curves which best fit the experimental points are shown as solid curves in Fig. 8. The A-exciton parameters obtained in this way are $\epsilon_0 = 8.4$, $M_\perp = 0.40 \pm 0.05 m_0$, $\omega_T = 14\,713 \pm 1$ cm^{-1}, and $\omega_L - \omega_T = 4 \pm 1$ cm^{-1}. Our value of ϵ_0 and $M_\perp$ are in good agreement with those of Kiselev *et al.*[34] Our value of ω_T is lower than theirs, probably because of the difference in sample temperatures (their sample temperature was 1.6 K). Their value of $\omega_L - \omega_T$ is almost double our value. There is no obvious explanation for this large discrepancy. Kiselev *et al.*[34] claimed an accuracy of ± 0.1 cm^{-1} in their determination of $\omega_L - \omega_T$, although we note that there are disagreements between their theoretical and experimental curves just between ω_T and ω_L. Also their reflectivity spectra are sensitive to the Γ_6 forbidden exciton and the additional boundary conditions while the Brillouin peak positions are not.

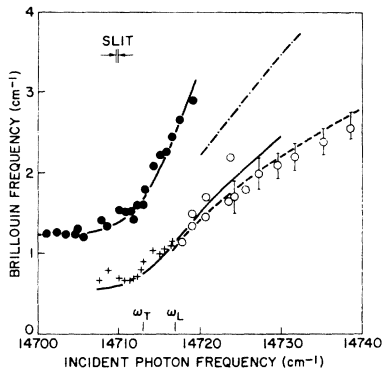

FIG. 8. Brillouin frequencies of CdSe-*P* plotted as a function of the incident laser frequency. The solid circles and the crosses correspond to the momentum-conserving LA and TA modes, respectively. The solid lines are theoretical fits to the experimental points using the polariton parameters listed in the text. The open circles correspond to the momentum-nonconserving modes. The broken curve is the calculated Brillouin frequency of the momentum-nonconserving TA* mode assuming that $M_\parallel = 1.3 m_0$. The dot-dashed curve is the calculated 2TA phonon frequency assuming that $M_\parallel = m_0$. This curve is presented to show that the open circles cannot be identified as two-phonon modes.

Figure 9 shows how the full widths at half maximum (γ) of the TA and LA peaks increase with ω_i, as predicted theoretically by Brenig *et al.*[11] According to this theory, γ is determined by the imaginary part of the incident- and scattered-polariton wave vectors (denoted by k_i'' and k_s'', respectively)

$$\gamma = 2v_s(k_i'' + k_s'') , \tag{4}$$

where v_s is the velocity of the acoustic phonon, and k_i'' and k_s'' are obtained by solving Eq. (2) with

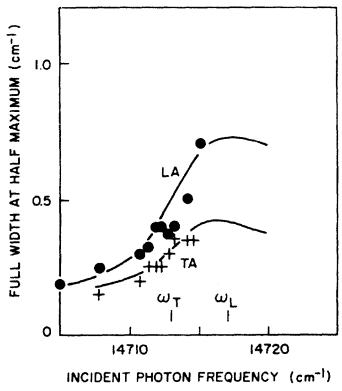

FIG. 9. Full width at half maximum of the TA (crosses) and LA (solid circles) modes in CdSe-*P* plotted as a function of the incident laser frequency. The solid curves are calculated from the polariton dispersion [Eq. (2)] using Eq. (4) and $\Gamma = 2$ cm^{-1}. The other polariton parameters in Eq. (2) are given in the text and are determined by the Brillouin frequencies in Fig. 8.

a nonzero damping Γ. Since all the exciton parameters have been fixed by the dispersion of the Brillouin peak frequencies, the experimental γ can be fitted with Eq. (4) by adjusting only Γ. For $\omega_i \ll \omega_T$, the Brillouin widths we measured are limited by the spectrometer resolution; we have therefore added to the theoretical γ a constant background of 0.16 cm^{-1}. The resultant theoretical curves for $\Gamma = 2$ cm^{-1} are shown as the solid lines in Fig. 9. The observed increases in γ around ω_T are in agreement with theory. We also note that Γ in CdSe-P is equal to Γ_e in CdSe as calculated from Eq. (3). This justifies our assumption of using a Γ equal to zero in fitting the Brillouin frequencies in Fig. 8.

For ω_i in the vicinity of ω_L, we found that the lower-frequency TA Brillouin peak started to broaden very fast and it persisted even for ω_i more than 20 cm^{-1} above ω_L, while the LA peak disappeared. A careful examination of the Brillouin spectra in this region (shown in Fig. 10) reveals that the low-frequency peak probably consists of at least two overlapping peaks [see, for example, curve (d) in Fig. 10]. We no longer identify the lower-frequency Brillouin peak in this region as due entirely to scattering of the TA phonon, which we did in a previous short communication (Ref. 25). This is the reason why Fig. 9 shows no data points for the TA mode above $\omega_i = 14\,715$ cm^{-1}, unlike Fig. 3 in Ref. 25. In Fig. 8, these new unidentified low-frequency peaks are shown as open circles, as distinct from the crosses for the TA mode.

In CdS, broad Brillouin peaks whose frequencies vary with ω_i for ω_i well above ω_L have been reported by both Winterling and Koteles[42] and by Yu and Evangelisti.[43] In CdS these peaks have been identified as two-phonon Brillouin modes. In order to test whether these broad peaks in CdSe-P are two-phonon modes or not, we have repeated the calculation of Yu and Evangelisti[43] using the CdSe polariton parameters derived from the one-phonon Brillouin modes. We found that for $M_{\parallel} \geq m_0$ all the two-phonon peaks in CdSe have frequencies much higher than that of the observed peak. As an illustration, we show in Fig. 8 the calculated frequencies of the 2TA mode in CdSe for $M_{\parallel} = m_0$ (dot-dashed curve). If we force the 2TA mode to have the same frequency as the observed peak, we have to assume that $M_{\parallel} = 0.2m_0$, which is not consistent with the result of Wheeler and Dimmock[27] nor with the result of the $\vec{k}\cdot\vec{p}$ calculation.[44] As a result, we propose that these broad dispersive Brillouin peaks are the TA* or LA* modes due to elastic exciton-defect scattering. This identification is supported by the fact that the properties of these peaks agree with those predicted by the theory of Gogolin and Rashba discussed in Sec. II B. For example, these peaks are broader than the one-phonon Brillouin peaks not involving defect scattering. They appear only for $\omega_i \gtrsim \omega_L$. Furthermore, with this identification the dependence of their peak frequencies on ω_i can be quantitatively explained. Although curves (c) to (f) in Fig. 10 indicate that there are two broad, dispersive peaks, we will concentrate on the stronger lower-frequency peak which we identify as TA*. From Fig. 2(c), the wave vector q of the TA phonon scattered is determined by ω_i through

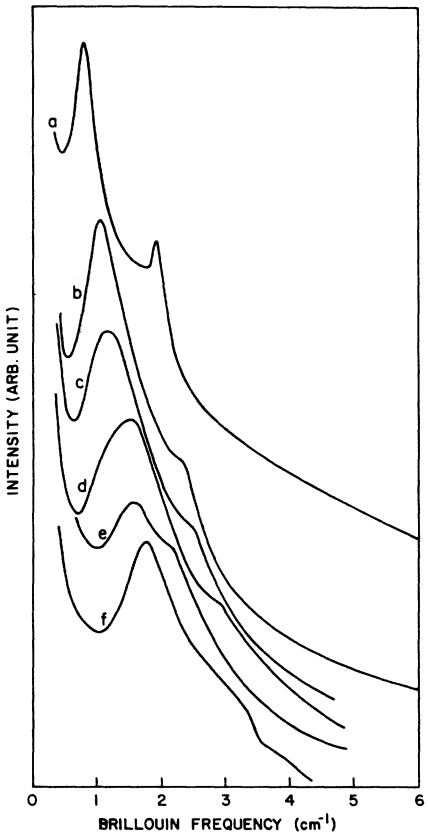

FIG. 10. Brillouin spectra of CdSe-P showing the appearance of the broad, momentum-nonconserving modes for incident photon frequencies above the longitudinal exciton frequency (14 717 cm^{-1}). The laser frequencies for the six curves are, respectively (a) 14 714.6, (b) 14 715.1, (c) 14 717.8, (d) 14 719, (e) 14 723.7, and (f) 14 725.7 cm^{-1}. In curve (a) the two sharp peaks are the TA and LA modes. These two peaks decrease in intensity with increase in ω_i, while new broad structures appear. In curves (c) and (d) the lower-frequency peak consists of two unresolved peaks which became separate in curves (e) and (f). The lower-frequency peak at around 1.8 cm^{-1} in curves (e) and (f) is identified as TA* (see text). The higher-frequency peak is difficult to identiy because it is much weaker.

$$\omega_i \simeq \omega_{ex}(0) + \tfrac{1}{2}\hbar q^2 \left(\frac{\cos^2\theta}{M_{\parallel}} + \frac{\sin^2\theta}{M_{\perp}}\right), \quad (5)$$

where θ is the angle between $\vec{q}$ and the c axis. In CdSe, as in CdS, the piezoelectric exciton-acoustic phonon interaction tends to be strongest for $\vec{q}$ almost parallel to the c axis,[43,20] so the frequency of the TA* mode is determined mainly by $M_{\parallel}$. The broken curve in Fig. 8 is obtained by adjusting $M_{\parallel}$ to be $1.3m_0$, a value consistent with the result of Wheeler and Dimmock[27] and with the result of the $\vec{k}\cdot\vec{p}$ band calculation.[44] The agreement between the theoretical curve and the experimental points is good. From the piezoelectric constants of CdSe, we expect the LA* mode to be comparable in intensity to the TA* mode. Thus it is not obvious why we do not observe the LA* mode. If we identify the lower-frequency peak in Fig. 8 as the LA* mode instead of the TA* mode, we will have to adjust $M_{\parallel}$ to be $0.85m_0$, a value too small to be consistent with the result of Wheeler and Dimmock.[27] Although there is another broad peak at higher frequency in curves (e) and (f) of Fig. 10, its position does not agree with that of the LA* mode. We have not been able to identify this peak.

B. Resonant Raman scattering in CdSe-P

Figure 11 shows several Raman spectra of CdSe-P for ω_i in the vicinity of ω_T and ω_L. In curve (a) ω_i is slightly below ω_T and the LO-phonon spectrum is quite similar to the nonresonant spectrum shown in Fig. 4. However, when ω_i is exactly resonant with ω_T [curve (b)], a fairly sharp peak appears at the Γ_1 (LO) phonon frequency of 212.3 cm^{-1}. This peak increases rapidly in intensity with increase in ω_i [curves (c) and (d)], while the Γ_5 (LO) peak becomes weaker. The intensities of the Γ_5 (LO) phonon and the 212.3-cm^{-1} peak are plotted as a function of ω_i in Fig. 12. Other than the peak at the bound exciton, the enhancement of the Γ_5 (LO) phonon for $\omega_i < \omega_L$ agrees qualitatively with the predictions of the polariton theory of resonant Raman scattering discussed in Sec. II A. This enhancement is also similar to what was observed by Koteles and Winterling in CdS.[20] However, for $\omega_i \gtrsim \omega_L$, significant differences show up between our CdSe result and the result of Koteles and Winterling.[20] In CdS, as the Γ_5 (LO) peak decreases in intensity, various two-phonon peaks due to an LO phonon plus an acoustic phonon appear and dominate the Raman spectra. In CdSe we do not observe any two-phonon peak but only the fairly sharp peak at 212.3 cm^{-1}. This peak cannot be identified as a two-phonon peak because its frequency does not change with ω_i. Instead, we find that the behaviors of this peak are all consistent with those of the momentum-nonconserving Γ_1 (LO*) mode.

First, in our scattering geometry of $\vec{k} \perp \vec{c}$, the Γ_1 (LO) phonon is not allowed by momentum conservation. Since the Γ_1 (LO*) mode is much stronger than the momentum-conserving Γ_5 (LO) mode, one may argue that a strong disorder oriented along the c axis may be responsible for this breakdown in momentum conservation. For example, breakdown in momentum conservation in resonant Raman scattering due to stacking

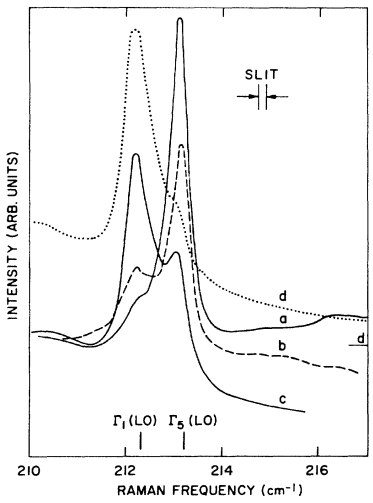

FIG. 11. Raman spectra of CdSe-P for four incident photon frequencies: (a) 14 704.9, (b) 14 712.8, (c) 14 716.5, and (d) 14 719 cm^{-1}. Curve (d) has been displaced upwards for clarity. The bar on the right-hand side marks its baseline. For all the curves, the scattering geometry is $\vec{E} \perp \hat{c}$ and $\vec{k} \perp \hat{c}$.

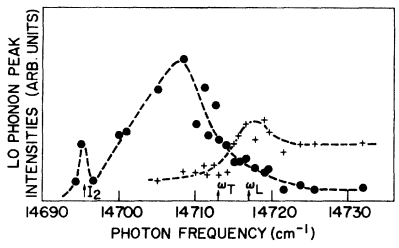

FIG. 12. The peak intensity of the Γ_5 (LO) phonon (solid circles) and the 212.3 cm^{-1} peak (crosses) in CdSe-P plotted as a function of incident photon frequencies. The broken curves are for guidance of the eye only.

faults has been reported in GaSe.[45] However, GaSe tends to form polytypes and is known to possess stacking faults,[46] while stacking faults are not known to exist in CdSe. Instead, the relative strength of the Γ_1 (LO*) and Γ_5 (LO) peaks can be explained within the theory of Gogolin and Rashba by the wave-vector dependence of the Fröhlich interaction and the anisotropy of the exciton mass in CdSe. From Fig. 2(c), the LO-phonon intensities are determined essentially by the rate of emission of LO phonons by the exciton-like branch 2 polariton. If $I_s(\omega_s)$ denotes the scattered intensity and $F(\vec{q})$ is the Fröhlich matrix element, for $\omega_i > \omega_L$, $I_s(\omega_s)$ is given approximately by

$$I_s(\omega_s) \propto \sum_{\vec{q}} F(\vec{q})\delta(\omega_i - \omega_s - \omega_{LO}(\vec{q})) . \quad (6)$$

It is important to include in Eq. (6) the anisotropy in the LO-phonon dispersion. The summation over $\vec{q}$ in Eq. (6) is subject to the condition imposed by Eq. (5). Since $F(\vec{q}) \propto q^2$ and $M_{\parallel} \gg M_{\perp}$ the Γ_1 (LO*) mode with $\vec{q} \parallel \hat{c}$ is much stronger than the Γ_5 (LO) mode with $\vec{q} \perp \hat{c}$. Using the value of $M_{\parallel} \simeq 1.3m_0$ deduced from the Brillouin data and assuming that the phonon density of states are approximately equal for the Γ_5 and Γ_1 modes we obtain $I_s(\Gamma_1)/I_s(\Gamma_5)$ should be ~3.6 for $\omega_i \gg \omega_L$. This value is in reasonable agreement with the experimental value of ~5 [curve (d) in Fig. 11].

The relative sharpness and enhancement of the 212.3-cm^{-1} peak are also consistent with the behavior of the momentum-nonconserving LO* phonon predicted by the theory of Gogolin and Rashba. Finally, we note that the appearance of the 212.3-cm^{-1} peak occurs approximately at the same incident photon frequencies as the TA* mode in the Brillouin spectra when ω_i becomes larger than ω_L. This is expected from Fig. 2(c).

To summarize our results in CdSe-P, we observe that for $\omega_i \lesssim \omega_T$ momentum is conserved in the Brillouin and Raman scatterings of polaritons. When ω_i is larger than ω_L we found that momentum is not conserved in both Brillouin and Raman scattering. This occurs as a result of elastic scattering between defects (presumably donors) in the sample and the polariton. The defects scatter polaritons in the photonlike branch 1 into the excitonlike branch 2. Because of the large exciton mass parallel to the c axis ($M_{\parallel}$) in CdSe, the polaritons propagating parallel to the c axis have much larger wave vectors. Since the Fröhlich and piezoelectric exciton-phonon interactions are both strongly wave-vector dependent, the $\vec{q} \parallel \hat{c}$ excitons scatter more strongly with phonons than the $\vec{q} \perp \hat{c}$ excitons. As a result, the scattered spectra are dominated by phonons with $\vec{q}$ parallel to the c axis and momentum is not conserved in the light-scattering process. The behaviors of these momentum-nonconserving modes are all consistent with the theoretical predictions of Gogolin and Rashba, thus providing strong evidence that elastic exciton-defect scattering is important in resonant Raman and Brillouin scattering in our CdSe sample.

C. Resonant Raman and Brilliouin scattering in CdSe-L

From the high impurity concentrations in CdSe-L and the absence of polariton effects in its reflectivity spectra, we do not expect to observe resonant Brillouin scattering in CdSe-L. However, we do observe two low-frequency peaks in CdSe-L and one of them we identify as a Brillouin peak.

Figure 13 shows several Brillouin spectra of CdSe-L at 2 K excited at laser frequencies in the vicinity of the A exciton: (a) 14 700.1, (b) 14 720.8, and (c) 14 722.0 cm^{-1}. The peak intensities and frequencies of the two modes in Fig. 13 are plotted as a function of incident laser frequencies in Fig. 14. From these figures, we observe that the low-

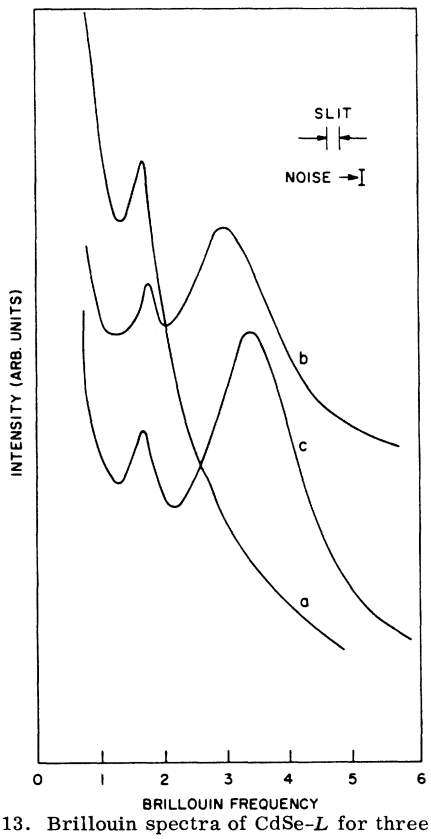

FIG. 13. Brillouin spectra of CdSe-L for three different excitation frequencies: (a) 14 700.1, (b) 14 720.8, and (c) 14 722.0 cm^{-1}. The higher-frequency peak in curves (b) and (c) is the one of interest in this paper. The sample temperature in this case is ~2 K.

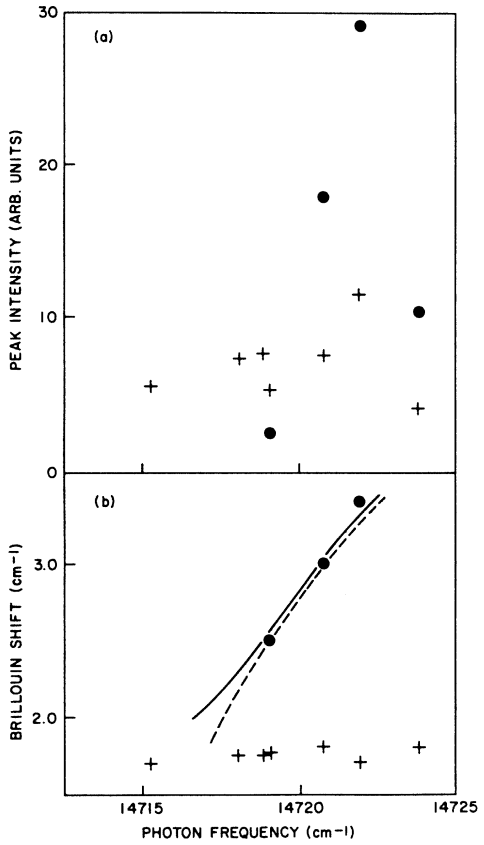

FIG. 14. Intensity and frequencies of the two peaks in the Brillouin spectra of CdSe-L plotted as a function of excitation wavelength. The solid circles and the crosses correspond respectively to the high- and low-frequency peaks.

frequency mode at ~1.8 cm^{-1} does not depend very much on the excitation wavelength. At the present time, we do not have a positive identification for this mode. Its frequency is very close to the β mode in Ref. 25 so it is probably an impurity-induced mode also.

We are more interested in the higher-frequency mode because both its frequency and intensity changes with excitation frequency. The sharp resonance in its intensity around the A exciton suggests that it involves the A exciton as a resonant intermediate state in its scattering process. The variation of its frequency with ω_i is very similar to the dispersive Brillouin modes in CdSe-P (Fig. 8). We have, therefore, identified this mode as a resonantly enhanced Brillouin mode in CdSe-L. We found that there are two possible Brillouin processes which are capable of explaining the peak frequencies of this mode. In one of the theories, this mode is identified as a 2TA mode. The peak frequencies of the 2TA mode can be calculated using the results of Yu and Evangelisti in Ref. 43. The experimental points (closed circles) in Fig. 14(b) can be fitted quite well by the calculated curve (solid curve) by adjusting $M_{\parallel}$ to be equal to m_0. However, this theory is not entirely satisfactory because $M_{\parallel}$ is smaller than the value $1.3m_0$ required to explain the Brillouin results in CdSe-P. Also, there is no reason why the 2TA mode is absent in the purer CdSe-P sample, while present in the dirtier CdSe-L sample. As an alternate explanation, we identify this mode as a momentum-nonconserving Brillouin mode. The larger amount of impurities in this sample justifies this identification. Using $M_{\parallel}$ equal to $1.3m_0$ obtained earlier, we found that the experimental peak frequencies all fall on the calculated curve for the LA* mode [broken curve in Fig. 14(b)]. Although the agreement between experiment and the second theory is quite good for the limited number of experimental points, this theory does not explain the appearance of the TA* mode in CdSe-P and the LA* mode in CdSe-L. One possible explanation could be that the different impurities contained by the two samples account for this difference.

The Raman scattering results in CdSe-L are qualitatively different from those of CdSe-P and can be understood in terms of the higher impurity concentration of CdSe-L. In Fig. 6, we have already shown that the Raman modes in CdSe-L are broader than in CdSe-P. Furthermore, the momentum-nonconserving Γ_1 (LO*) mode is always present in the $\vec{k} \perp \hat{c}$ and $\vec{E} \parallel \hat{c}$ configuration even for ω_i below ω_T. We note that in CdSe-P the Γ_1 (LO*) mode is not significant for ω_i below ω_T, but becomes dominant for ω_i above ω_L. In CdSe-L

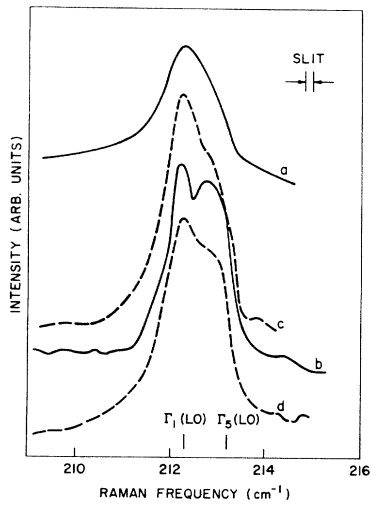

FIG. 15. Raman spectra of CdSe-L measured in the configuration $\vec{E} \perp \hat{c}$ and $\vec{k} \perp \hat{c}$ for different incident photon frequencies: (a) 14 706.3, (b) 14 715.2, (c) 14 719.1, and (d) 14 723.8 cm^{-1}.

we found that the Γ_1 (LO*) mode is always stronger than the Γ_5 (LO) mode and its intensity does not change much with ω_i. This is clear from Fig. 15, where four Raman spectra of CdSe-L for four different ω_i's are compared. The value of ω_i for curves (a), (b), (c), and (d) in Fig. 15 are, respectively, 14706.3, 14715.2, 14719.1, and 14723.8 cm^{-1}.

The above results in CdSe-L can be explained qualitatively by its higher impurity concentration. The impurities broaden the LO phonons by shortening their lifetime and increase the probability of exciton-impurity scattering. In the purer CdSe-P sample, exciton-impurity scattering is important only for $\omega_i > \omega_L$ when real exciton intermediate states can be excited. In CdSe-L, the amount of impurities is presumably large enough that exciton-impurity scatterings via virtual-exciton states (these states can be free or bound) are also important. These scatterings account for the presence of the momentum-nonconserving Γ_1 (LO*) mode for $\omega_i < \omega_T$ when only virtual-exciton intermediate states are excited.

VI. CONCLUSION

We have studied resonant Raman and Brillouin scattering in CdSe with a dye laser and spectrometer system whose combined spectral width is ~0.16 cm^{-1}. We have observed changes in the Raman and Brillouin line shapes of CdSe with excitation frequency. In a nominally undoped CdSe sample we found that, for laser frequencies below the A-exciton frequency, momentum is conserved in both Raman and Brillouin scattering. Applying the theory of Brenig *et al.* for Brillouin scattering by exciton polaritons, we deduced the polariton parameters in CdSe. When the laser frequencies are above the exciton frequency, we found that both the Brillouin and Raman spectra in our CdSe sample become dominated by momentum-nonconserving peaks. We propose that these peaks are caused by elastic exciton-defect scatterings and our results are in qualitative agreement with the theory of Gogolin and Rashba. In a more heavily doped CdSe sample, we found that momentum is not conserved in light scattering even for laser frequencies below the exciton frequency. This is consistent with the higher impurity concentration in this sample resulting in stronger exciton-defect scattering.

Our results in CdSe support the contention of Gogolin and Rashba that even small amounts of crystal defects, such as impurities, play an important role in resonant light scattering. The reason is that elastic exciton-defect scatterings produce momentum-nonconserving modes whose resonance enhancements are different from those of the momentum-conserving modes. In anisotropic crystals, such as CdSe, we were able to separate the momentum-conserving Raman modes from the nonconserving ones by their different frequencies. This is not always possible, especially in cubic crystals, and the effect of impurities has to be taken into consideration in analyzing resonant Raman scattering results.

ACKNOWLEDGMENTS

We are grateful to Dr. Y. Petroff of LURE, Orsay; Dr. D. C. Reynolds of Wright Patterson Air Force Base and Dr. P. W. Yu of the University of Dayton for providing us with CdSe samples. We are also indebted to Dr. J. Kuptsis for performing the spark-source mass-spectroscopy analyses and to J. A. Bradley for his expert technical assistance.

*Present address: Laboratoire de Physique de la Matière Condensée, Ecole Polytechnique, 91128, Palaiseau, France.

†Present address: Physics Department, University of California, Berkeley, California 94720.

[1]See, for example, A. S. Barker, Jr., and A. J. Sievers, Rev. Mod. Phys. 47, S1 (1975); in *Localized Excitations in Solids*, edited by R. F. Wallis (Plenum, New York, 1978); in *Light Scattering in Solids*, edited by M. Balkanski (Flammarion, Paris, 1971).

[2]J. M. Worlock and S. P. S. Porto, Phys. Rev. Lett. 15, 697 (1965); D. J. Evans and S. Ushioda, Phys. Rev. B 9, 1638 (1974); S. Ushioda, Solid State Commun. 15, 149 (1974); A. Compaan, *ibid.* 16, 293 (1975); R. L. Farrow, R. K. Chang, and R. M. Martin, in *Physics of Semiconductors, 1978*, edited by B. L. H. Wilson (Institute of Physics and Physical Society, London, 1979), p. 485.

[3]P. Y. Yu, M. H. Pilkuhn, and F. Evangelisti, Solid State Commun. 25, 371 (1978); P. Y. Yu, Phys. Rev. B 20, 5286 (1979).

[4]J. F. Scott, R. C. C. Leite, and T. C. Damen, Phys. Rev. 188, 1285 (1969); P. J. Colwell and M. V. Klein, Solid State Commun. 8, 2095 (1970); in *Light Scattering in Solids*, edited by M. Balkanski (Flammarion, Paris, 1971), p. 65; P. F. Williams and S. P. S. Porto, *ibid.* p. 70; T. C. Damen and J. Shah, Phys. Rev. Lett. 27, 1506 (1971).

[5]P. Yu and Y. R. Shen, in *Proceedings of the Twelfth International Conference on the Physics of Semiconductors, Stuttgart, 1974*, edited by M. H. Pilkuhn (Teubner, Stuttgart, 1974), p. 453.

[6]S. Permogorov and A. Reznitsky, Solid State Commun. 18, 781 (1976).

[7]R. Ulbrich and C. Weisbuch, private communication.

[8]A. K. Ganguly and J. L. Birman, in *Light Scattering*

Spectra of Solids, edited by G. B. Wright (Springer, New York, 1968), p. 487.
[9]A. A. Gogolin and E. I. Rashba, Solid State Commun. 19, 1177 (1976).
[10]See, for example, R. M. Martin and L. M. Falicov, in *Light Scattering in Solids*, edited by M. Cardona (Springer, Heidelberg, 1976) and references therein.
[11]W. Brenig, R. Zeyher, and J. L. Birman, Phys. Rev. B 6, 4617 (1972).
[12]P. Y. Yu, in *Excitons*, edited by K. Cho (Springer, Heidelberg, 1979), p. 211.
[13]J. J. Hopfield, Phys. Rev. 112, 1555 (1958).
[14]W. C. Tait, Phys. Rev. B 5, 648 (1972).
[15]See, for example, R. Ulbrich and C. Weisbuch, Phys. Rev. Lett. 38, 865 (1977); in *Festkörperprobleme (Advances in Solid State Physics)*, edited by J. Treusch (Vieweg, Braunschweig, 1978), Vol. XVIII, p. 217.
[16]E. Burstein, D. L. Mills, A. Pinczuk, and S. Ushioda, Phys. Rev. Lett. 22, 348 (1969).
[17]L. N. Ovander, Fiz. Tverd. Tela (Leningrad) 3, 2394 (1961) [Sov. Phys. Solid State 3, 1737 (1962)]; 4, 1471 (1962) [4, 1081 (1962)]; and E. M. Verlan and L. N. Ovander, *ibid.* 8, 2435 (1966) [*ibid.* 8, 1939 (1967)].
[18]B. Bendow and J. L. Birman, Phys. Rev. B 1, 1678 (1970); B. Bendow, *ibid.* 2, 505 (1970); 4, 552 (1971).
[19]J. J. Hopfield, Phys. Rev. 182, 945 (1969).
[20]E. S. Koteles and G. Winterling, Phys. Rev. B 20, 628 (1979).
[21]C. Hermann and P. Y. Yu (unpublished).
[22]A. A. Gogolin, Fiz. Tverd. Tela (Leningrad) 15, 2746 (1973) [Sov. Phys. Solid State 15, 1824 (1974)].
[23]V. I. Sugakov, Opt. Spektrosk. 24, 477 (1968) [Opt. Spectros. (USSR) 24, 253 (1968)]; 26, 732 (1969) [26, 401 (1969)].
[24]J. J. Hopfield, in *Proceedings of the International Conference on the Physics of Semiconductors, Exeter, 1962* (The Institute of Physics and The Physical Society, London, 1962), p. 75.
[25]C. Hermann and P. Y. Yu, Solid State Commun. 28, 313 (1978).
[26]R. B. Parsons, W. Wardzynski, and A. D. Yoffe, Proc. R. Soc. London A 262, 120 (1961).
[27]R. G. Wheeler and J. O. Dimmock, Phys. Rev. 125, 1805 (1962).
[28]D. W. Langer, R. N. Euwema, K. Era, and T. Koda, Phys. Rev. B 2, 4005 (1970).
[29]V. A. Kiselev, B. S. Razbirin, and I. N. Ural'tsev, Pis'ma Zh. Eksp. Teor. Fiz. 18, 504 (1973) [JETP Lett. 18, 296 (1973)].
[30]E. F. Gross, B. S. Razbirin, V. P. Fedorov, and Yu. P. Naumov, Phys. Status Solidi 30, 485 (1968).
[31]D. C. Reynolds, C. W. Litton, and T. C. Collins, Phys. Rev. 156, 881 (1967).
[32]C. H. Henry, K. Nassau, and W. Shiever, Phys. Rev. B 4, 2453 (1971).
[33]B. Segall, in *Physics and Chemistry of II-VI Compounds*, edited by M. Aven and J. S. Prener (North-Holland, Amsterdam, 1967).
[34]V. A. Kiselev, B. S. Razbirin, and I. N. Ural'tsev, Phys. Status Solidi B 72, 161 (1975).
[35]V. G. Plotnichenko, Yu. A. Mityagin, and L. K. Vodop'yanov, Fiz. Tverd. Tela (Leningrad) 19, 2703 (1977) [Sov. Phys. Solid State 19, 1584 (1977)].
[36]D. Berlincourt, H. Jaffe, and L. R. Shiozawa, Phys. Rev. 129, 1009 (1963).
[37]R. Loudon, Adv. Phys. 14, 621 (1965); R. A. Arguello, D. L. Rousseau, and S. P. S. Porto, Phys. Rev. 181, 1351 (1969).
[38]See, for example, J. F. Nye, *Physical Properties of Crystals* (Oxford University Press, London, 1969).
[39]G. Winterling, E. S. Koteles, and M. Cardona, Phys. Rev. Lett. 39, 1286 (1977).
[40]P. A. Temple and C. E. Hathaway, Phys. Rev. B 7, 3685 (1973); B. A. Weinstein and M. Cardona, Solid State Commun. 10, 961 (1972).
[41]P. Y. Yu, in *Light Scattering in Solids*, edited by M. Balkanski, R. C. C. Leite, and S. P. S. Porto (Flammarion, Paris, 1976), p. 19; Solid State Commun. 19, 1087 (1976); in *Physics of Semiconductors*, edited by F. G. Fumi (Tipogravia Marves, Rome, 1976), p. 235.
[42]G. Winterling and E. S. Koteles, in *Lattice Dynamics*, edited by M. Balkanski (Flammarion, Paris, 1978), p. 170.
[43]P. Y. Yu and F. Evangelisti, Solid State Commun. 27, 87 (1978).
[44]M. Cardona, J. Phys. Chem. Solids 24, 1543 (1963).
[45]R. M. Hoff and J. C. Irwin, Phys. Rev. B 10, 3464 (1974).
[46]J. C. J. M. Terbell and R. M. A. Lieth, J. Cryst. Growth 16, 54 (1974).